LIGO SURF Proposal
Improved Targeted sub-threshold Search for Strongly Lensed Gravitational Waves with Sky Location Constraint

Aidan H.Y. Chong,[1, a]
Mentors: Alvin Li,[2, b] Ryan Magee,[2, c] Juno. C.L. Chan,[1, d] Cody Messick,[3, e] and Alan J. Weinstein[2, f]

[1]*Department of Physics, The Chinese University of Hong Kong*
[2]*LIGO Laboratory, California Institute of Technology*
[3]*LIGO Laboratory, Massachusetts Institute of Technology*

(Dated: April 2022)

Gravitational lensing is an important field in both astrophysics and cosmology as it could provide a large amount of crucial information about our universe unmatched by other phenomena. Until recently, gravitational lensing had only been applied to the observation of the electromagnetic spectrum. Since the first successful observation of gravitational waves back in 2015, discussions had started to try to find lensed gravitational wave signals. However, in most cases, the lensed image should be much dimmer, which might be buried in the noise as it could not pass the normal detection threshold. Our work would be to modify the existing GstLAL searching pipeline to suit our need for lensing searches. We hope to recover originally buried sub-threshold lensed signal from the collected data. Our searches would cover data from all 3 observation runs in LIGO and VIRGO.

I. INTRODUCTION

Gravitational waves, predicted by Albert Einstein's theory of General Relativity proposed in 1915 [1], were first detected by LIGO (**L**aser **I**nterferometer **G**ravitational-Waves **O**bservatory) in 2015 [2]. Since then, more than 90 gravitational waves from compact binary coalescences have been detected in the three observing runs [3] [4] [5] [6]. Gravitational waves open a new window for us to study the universe, which allows us to fine-tune the modelling of neutron stars [7] [8] [9], understand the formation channels of astrophysical objects [7] [10], study the early universe using the stochastic background [11] [12] and find out the expansion rate of the universe by measuring the Hubble's parameter [13] [14].

General relativity dictates that massive objects can curve spacetime, and hence when light passes by massive objects, its path will be refracted and deflected before reaching the observer, while being magnified or demagnified, hence forming multiple images arriving at different times. Such phenomenon is known as gravitational lensing. Gravitational lensing is widely applied in astrophysics and cosmology. A gravitational lens can give information on the image source, the object acting as the lens, and mostly importantly the intervening large-scale geometry of the universe in which the source, object, and the observer are at cosmological distances from each other [15]. From the equivalence principle, gravitational waves should be lensed in the same way. Since the first detection of gravitational waves, many efforts have been made to claim ,and dis-claim of observing lensed gravitational waves have been made [16] [17] [18]. To this date, there is not enough compelling evidence to show lensed pairs in the catalog of confirmed gravitational wave events [19].

Due to the sheer amount of data collected in multiple observing runs, we could not analyse all of the data collected as it would be too computationally costly. Instead, we only choose to analyse signals that pass certain detection threshold. The thresholds used are usually intensity thresholds, which measures how intense the collected signal is. In other words, if a signal has a signal-to-noise ratio (SNR) greater than a certain threshold value, it would produce a trigger. We would then perform analyses on the triggers utilising statistical parameters such as likelihood ratio to determine how likely it would be a true gravitational wave signal. Currently available pipelines for such searching of triggers includes GstLAL [20], MBTA [21], SPIIR [22] and PyCBC [23]. However, it is easy to see that for some real gravitational wave signals with relatively low intensities, either due to the source being too far away from Earth or demagnified by gravitational lensing, would simply be discarded as noise without producing a trigger. These low-intensity signals are called sub-threshold signals. Recovering these sub-threshold signals is important for lensing searches as we expect different lensed images will have different intensities, and some would be in the sub-threshold category.

While lensed images have different sky locations, the deviation (of the order of arc-seconds) is much smaller than the accuracy of the sky location inferred for sources of gravitational waves (in order of degrees), and hence we can treat lensed gravitational waves as if they are coming from the same sky location. In this research, we aim to further improve the sensitivity of the targeted search for sub-threshold lensed gravitational waves by including the extra constraint that they have to come from the same sky location as the target.

[a] 1155160056@link.cuhk.edu.hk
[b] kli7@caltech.edu
[c] ry.m.magee@gmail.com
[d] clchan@phy.cuhk.edu.hk
[e] cmessick@mit.edu
[f] ajw@caltech.edu

This paper is structured as follows. Section II presents the important background knowledge related to our research. Section III provides the method used in this research. Lastly, a work plan would be provided in section IV.

II. BACKGROUND

A. Physics of Gravitational Waves

Einstein's theory of General Relativity treated time as a spatial dimension, so together with 3D space, they constitute 4D spacetime. Einstein's field Equation is the equation responsible for giving the relationship between the motion of masses and the curvature of space-time. Mathematically speaking, the equation is written as[1]

$$R_{\mu\nu} - \frac{1}{2}Rg_{\mu\nu} = 8\pi T_{\mu\nu}, \tag{1}$$

where $R_{\mu\nu}$ is the Ricci tensor, R is Ricci scalar,$g_{\mu\nu}$ is the metric tensor and $T_{\mu\nu}$ is the Energy-Momentum tensor. From the equation, we can easily observe that the left-hand side represents the curvature of space-time and the right-hand side represents the energy and momentum of the object. As a result, mass in space-time would affect the curvature of the space-time around it.

From Einstein's field Equation, we can see that masses can warp spacetime. When a nonspherical and nonuniform mass is in motion, it produces ripples of curved spacetime. [15]. According to special relativity, the speed of causality is equal to the speed of light c [24], which means no signal could be transmitted faster than the speed of light, not even gravity. In this case, general relativity predicts that the speed of gravity, which also includes the propagating speed of gravitational waves would be travelling at the speed of light. Multi-messenger observation of GW170817 binary neutron star event has constrained the difference between the speed of gravity and the speed of light to be between -3×10^{-15} and $+7 \times 10^{-16}$ times the speed of light [7] [25], which is very close to the theoretical value. There are many sources of gravitational waves in our universe, including compact binary coalescence (CBC), supernova explosions, and the big bang [15]. Sadly, to this date, we have only confirmed to detect gravitational waves from CBC. For that reason, this research would only focus on gravitational waves emitted by CBC.

The curvature of spacetime is embedded in the metric tensor. For a flat spcaetime without curvature (Minkowski spacetime), the metric of flat spacetime is given by

$$g_{\alpha\beta}(x) = \eta_{\alpha\beta}, \tag{2}$$

[1] Units of c = G = 1 would be used throughout the report

where g is the metric and

$$\eta_{\alpha\beta} = \begin{bmatrix} -1 & 0 & 0 & 0 \\ 0 & 1 & 0 & 0 \\ 0 & 0 & 1 & 0 \\ 0 & 0 & 0 & 1 \end{bmatrix}. \tag{3}$$

When a small amplitude gravitational plane wave propagates through the cosmos towards Earth, the spacetime where the wave travels through can be approximated to be a flat spacetime (Minkowski spacetime) with very high accuracy [15]. We consider adding a small perturbation term $h_{\alpha\beta}$ to flat spacetime (with $|h_{\alpha\beta}| = 1$), such that the metric now becomes

$$g_{\alpha\beta}(x) = \eta_{\alpha\beta} + h_{\alpha\beta}(x), \tag{4}$$

where $h_{\alpha\beta}(x)$ is the small perturbations to the flat space-time metric, and we expand Einstein's field equation to the linear order of $h_{\alpha\beta}$, we will arrive at

$$\Box^2 h_{\alpha\beta} = -16\pi T_{\alpha\beta}. \tag{5}$$

For the region outside the source of gravitational waves, it is approximately a vacuum. Therefore, $T_{\alpha\beta} = 0$ in the space outside the source. Hence we have

$$\Box^2 h_{\alpha\beta} = 0, \tag{6}$$

which allows a plane-wave solution.

In the traceless-transverse (TT) gauge, the perturbation term of a gravitational wave travelling in the z-direction can be written as

$$h^{\mathrm{TT}}_{\alpha\beta}(t,z) = \begin{bmatrix} 0 & 0 & 0 & 0 \\ 0 & h_+ & h_\times & 0 \\ 0 & h_\times & -h_+ & 0 \\ 0 & 0 & 0 & 0 \end{bmatrix} \cos(t-z), \tag{7}$$

Where h_+ and $h_\times$ are the plus and cross-polarization content respectively. When the gravitational wave passes through a ring of test masses placed on the $x-y$ plane, it deforms the ring of test masses according to the polarization of the wave, as shown figure 1.

B. Detection of Gravitational Waves

Currently, all the detected gravitational waves were produced by the merger of massive and dense bodies such as black holes and neutron stars. When the 2 bodies clash with each other, space-time will be heavily distorted and the weak field approximation breaks down. Numerical simulations must be employed to find out the waveform in those situations.

The typical waveform of gravitational waves could be classified into 3 stages. The positions of the 3 stages were illustrated in figure 2. The inspiral and Ringdown stages could use perturbation theories to find approximated solutions but the merger stage could only be calculated using numerical

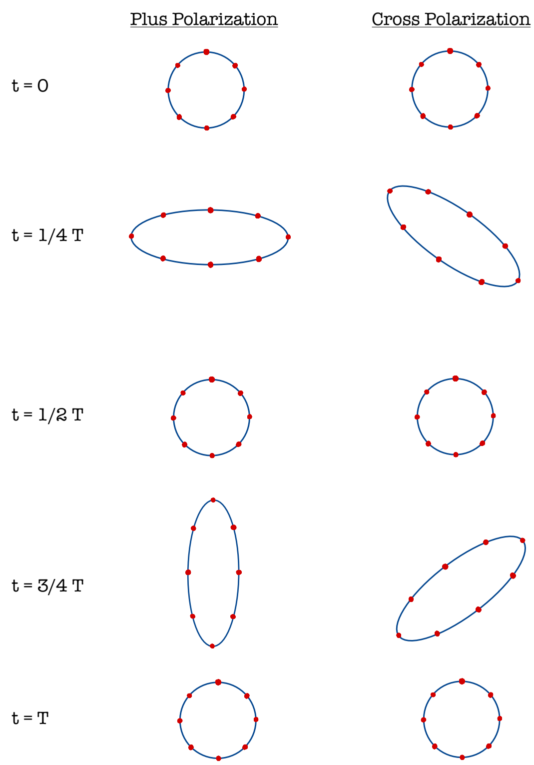

Figure 1. The behaviour of test masses under the influence of gravitational waves of different polarization. The period is T and t is the time since the beginning of the period. When a plus polarized gravitational wave propagates through spacetime, the test masses stretch in 2 perpendicular direction that together looks like a "+" shape, while for cross polarization it looks like a "×" shape

simulation.

The LIGO-Virgo-KAGRA (LVK) collaboration has altogether four detectors, in Hanford, Livingston, Europe, and Japan. At the time of writing, VIRGO in Europe and KARGA in japan are already operating. The detectors are Michaelson interferometers [26] with similar working principles as the detectors of LIGO with minor differences in their designs. Figure 3 shows the schematic diagram of a LVK gravitational-wave detector. The entire setup is placed inside a vacuum to reduce the thermal noise caused by the Brownian motion of air molecules and to reduce the probability of dust molecules blocking the path of light or sticking to the mirrors themselves [27], which would hinder the accuracy of the detector. The arm length L is set to be 4km long. The reason for constructing such a long arm is to elevate the sensitivity of the detector [28], although an effective distance of 4km is still not enough for gravitational wave detection. There are more technologies used by LIGO to further increase the sensitivity, which would be introduced later in this section. The laser used by LIGO is a 4W Laser light at 808nm [29] [27] [2] [3]. This near-infrared laser beam will then stimulate the emission of a 2W beam at a wavelength of 1064nm. The beam will later be amplified to 200W, this beam would be sent into

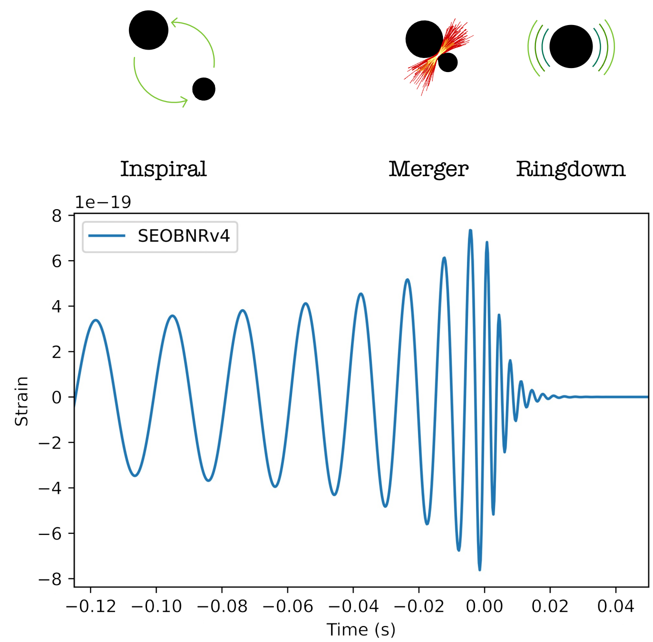

Figure 2. Top: Illustrations of the inspiral, merger, and ringdown stage of a compact binary coalescence. Bottom: A simulation plotted using pycbc. The gravitational wave was idealized without any noise to show the shape of the wave. On top of the plot are 3 illustrations of the merging black holes corresponding to each stage. (This graph would be changed to LAL sim in the later work)z

the detector. To reach the detection requirement of 750kW, power recycling mirrors were introduced. Inside each arm (between the power recycling mirror and the mirror), the laser beam is recycled about 300 times to pump up the effective power [28]. This recycling would also pump up the effective travelling length, which enlarged the distance travelled from 4km to 1200km. LIGO detectors also employed both active and passive vibration isolation systems [30] to try to reduce the noise to a minimal amount, such as optics suspension and seismic isolation. All these factors contribute to the fact that current detectors could attain sensitivities of at least 10^{-19}m to detect incoming gravitational waves. The noise budgets and sensitivities of the advanced LIGO (aLIGO) detectors are presented in figure 4.

The beam splitter, mirrors, and power recycling mirror are all attached to test masses [32]. These test masses are free to swing in the horizontal directions. When gravitational waves incident normally on the plane of the interferometer arms, one arm would be stretched while the other one would be contracted. Mathematically, if

$$\Delta L = L_x - L_y = n\lambda, \quad (8)$$

with L_x and L_y representing the arm length of the 2 arms, n = 0,1,2,3... and λ is the wavelength of light passing into the detector, then constructive interference would occur. On the

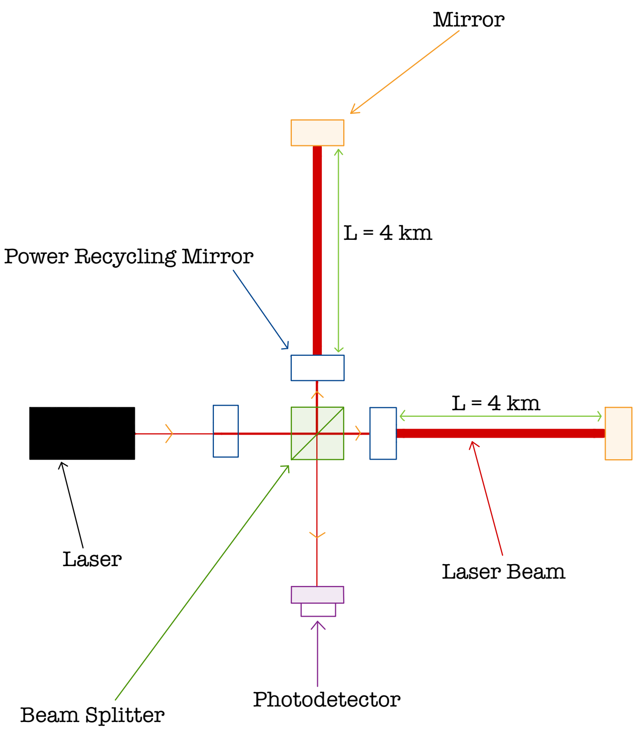

Figure 3. A schematic diagram of the LIGO detectors

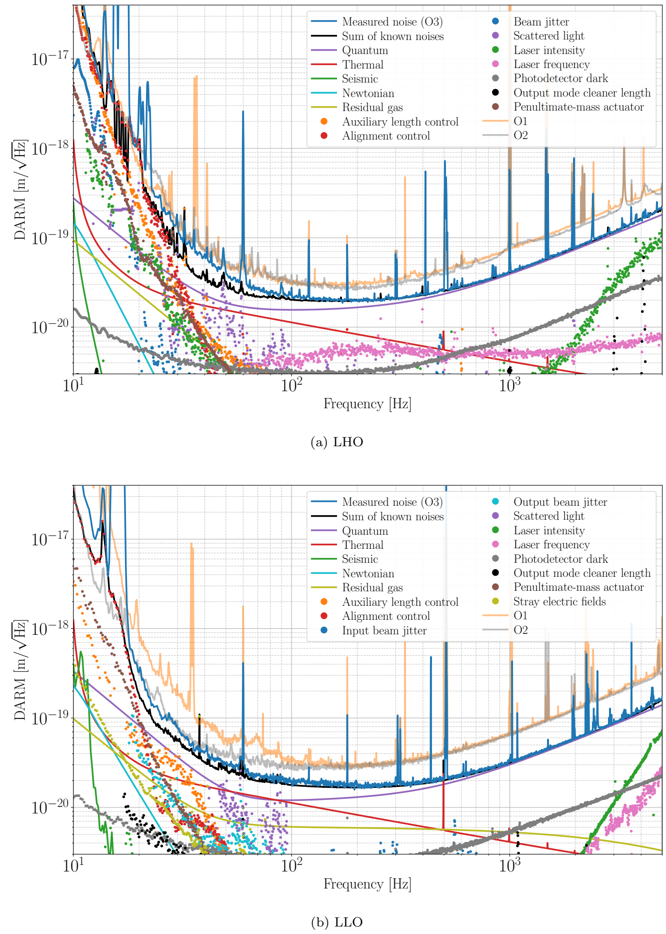

Figure 4. Full noise budget of (a) LIGO Handford Observatory (LHO) and (b) LIGO Livingston Observatory (LLO) [31]. The calculated noise terms are given in solid lines, while measured contributions are given as dots.

other hand if

$$\Delta L = L_x - L_y = (n + \frac{1}{2})\lambda, \tag{9}$$

destructive interference would occur. Any value of n between these 2 cases would lie between destructive and constructive interference.

C. Searching and Data Analysis of Gravitational Waves

While many methods were employed to reduce noise in the detectors, the noise in the collected data is usually very large. To successfully retrieve the real gravitational wave signal from all the noises, a technique called matched filtering could be used. In a nutshell, matched filtering considers the correlation between the data and the template waveforms. If a real gravitational wave is present in the data, the correlation between the two should be very high given that the template matches the real gravitational wave and the amplitude should not be too small.

After the 2 hypotheses we need to consider [33]:

1. Null hypothesis $\mathcal{H}_0$: There is only noise, so that $s(t) = n(t)$.

2. Signal hypothesis $\mathcal{H}_1$: There are both noise and signal, so that $s(t) = n(t) + h(t)$

Where $s(t)$ is the signal recorded, n(t) is the background noise and h(t) is the gravitational wave signal.

Define inner product as

$$(a, b) = 4Re \int_0^\infty \frac{\tilde{a}(f)\tilde{b}^*(f)}{S(f)} df. \tag{10}$$

Then the signal to noise ratio (SNR) could be expressed as

$$\rho = \frac{(d, h)}{\sqrt{(d, h)}}, \tag{11}$$

with d(t) representing the template waveform.

If it is assumed that the noise is Gaussian, it would be possible to compute the probability density. Under $\mathcal{H}_0$, we have $n(t) = s(t)$, and so

$$p(s|\mathcal{H}_0) = p_n[s(t)] \propto e^{-\frac{(s,s)}{2}}. \tag{12}$$

Under $\mathcal{H}_1$, we have $n(t) = s(t) - h(t)$, and so

$$p(s|\mathcal{H}_1) = p_n[s(t) - h(t)] \propto e^{-\frac{(s-h,s-h)}{2}}. \tag{13}$$

A new parameter called the likelihood ratio can be defined by the odd ratio for the alternative hypothesis given the observed data $s(t) = O(\mathcal{H}_1|s)$. Mathematically, it is written as:

$$\mathcal{L}(\mathcal{H}_1|s) = \frac{p(s|\mathcal{H}_1)}{p(s|\mathcal{H}_0)}, \tag{14}$$

where p is the probability density. Therefore we have,

$$\begin{aligned}\mathcal{L}(\mathcal{H}_1|s) &= \frac{e^{-\frac{(s-h,s-h)}{2}}}{e^{-\frac{(s,s)}{2}}}. \\ &= e^{s,h}e^{-\frac{(h,h)}{2}}\end{aligned} \tag{15}$$

It could be observed that the likelihood ratio depends on s(t) only through the inner product (s,h). The inner product

$$(s,h) = 4Re\int_0^\infty \frac{\tilde{s}(f)\tilde{h}^*(f)}{S(f)}df \tag{16}$$

is called the matched filter as it is a noise-weighted correlation of the anticipated signal with the data.

In reality, the likelihood ratio depends on many parameters [34] [20]. Therefore, it could be written explicitly as

$$\mathcal{L} = \frac{P(\vec{D}_H, \vec{O}, \vec{\rho}, \vec{\xi^2}, [\Delta\vec{t}, \Delta\vec{\phi}]|\vec{\theta}, \text{signal})}{P(\vec{D}_H, \vec{O}, \vec{\rho}, \vec{\xi^2}, [\Delta\vec{t}, \Delta\vec{\phi}]|\vec{\theta}, \text{noise})} \cdot \frac{P(\vec{\theta}|\text{signal})}{P(\vec{\theta}|\text{noise})}. \tag{17}$$

It can be observed that the likelihood ratio depends on:

1. Participating detectors $\vec{O}$.
2. Horizontal distances and hence the sensitivity of the detectors $\vec{D}_H$.
3. Matched filter Signal-to-Noise ratio (SNR) $\vec{\rho}$.
4. Signal consistency test value at each detector $\vec{\xi^2}$.
5. Time delay $\Delta\vec{t}$ (only for coincident events)
6. Phase delay $\Delta\vec{\phi}$ (only for coincident events)
7. The parameters of the templates $\vec{\theta}$

In practice, the value of $\mathcal{L}$ could be very large or very small. Therefore, $ln\mathcal{L}$ is usually used instead of $\mathcal{L}$ alone. After the search, a list of candidates would be ranked according to the $ln\mathcal{L}$ value.

False-alarm-probability (FAP) is the probability of pure noise to produce a trigger with a ranking statistic $ln\mathcal{L}$ larger or equal to the ranking statistic of the trigger $ln\mathcal{L}^*$. Mathematically, FAP could be written as

$$\text{FAP} = P(ln\mathcal{L} \geq ln\mathcal{L}^*|\text{noise}) = \int_{ln\mathcal{L}^*}^\infty P(ln\mathcal{L}|\text{noise})d(ln\mathcal{L}). \tag{18}$$

A low FAP means the probability of the signal being generated by pure noise is low, and vice versa. FAP is important to know as it is essential for calculating False-Alarm-Rate (FAR). FAR is another parameter used to compute the rate that how often would a pure noise produce a trigger with a ranking statistic $ln\mathcal{L}$ larger or equal to the ranking statistic of the trigger $ln\mathcal{L}^*$. Mathematically, FAR could be computed as

$$\text{FAR} = \frac{N \times \text{FAP}}{T}, \tag{19}$$

where N is the total number of observed candidates, T is the duration of the data analyzed. In short, the higher the FAR, the lower the likeliness that the recorded event is a gravitational wave event, and vice versa.

After all these procedures, the final list of ranked candidates would be transferred to analysts for further analysis such as using Bayesian methodology and posterior overlap analysis on the waveform [35]. If the event passed the analysis, it would be designated to be a new gravitational wave event.

Although in theory gravitational waves could be produced from other sources other than binary coalescence, the current sensitivity of our available detectors could only detect gravitational waves with relativity large amplitude (10^{-21}m) [26]. Therefore, gravitational waves from other sources are not readily detectable by contemporary detectors. As a result, this research would only focus on the lensing of gravitational waves from compact binary coalescence.

Research focusing on searching gravitational waves signal has developed numerous search pipelines to search for possible candidates. It was already mentioned that there are already numerous researches out there to search for gravitationally lensed counterparts of confirmed gravitational wave signals. However, it is confirmed that there are currently no gravitationally lensed pairs in the catalog of detected gravitational waves [19]. To find other possible lensed pairs, it is required to search for signals with a lower signal-to-noise ratio that usually would not cause a trigger during the search as the first detected lensed image would most probably be a sub-threshold signal [19]. These possible gravitational wave signals are called sub-threshold gravitational waves as their intensities are not high enough to reach the normal trigger threshold.

As mentioned before, this research employs GstLAL as our search pipeline. GstLAL is a pipeline originally built for gravitational waves detection but not gravitational waves.

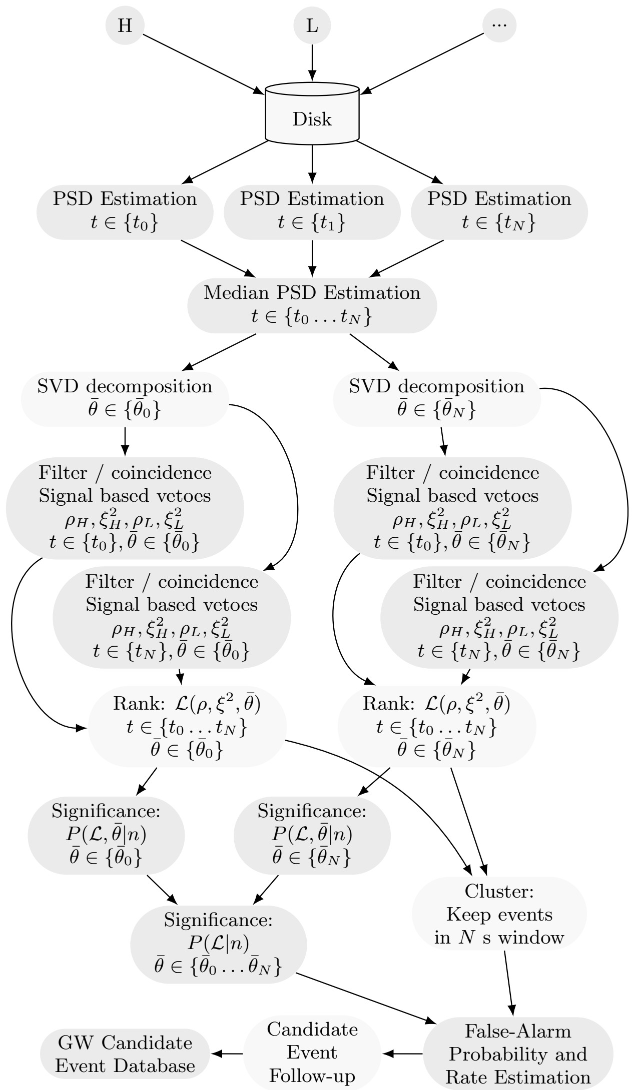

Figure 5. A flowchart of GstLAL pipeline [36]

However, it is possible for us to modify the pipeline to suit our requirement for sub-threshold gravitational lensing searching.

GstLAL is a gravitational wave signal searching pipeline that utilises matched-filtering analysis technique. The matched-filtering techniques is already mentioned in the previous section. The output of the matched-filter is the signal-to-noise ratio (SNR) [20], which is equivalent to the inner product of the whitened data with the whitened template. Whitening is required as there are always several strong spectral lines exist which would severely affect the data analysis process. In GstLAL pipeline, the calculations are performed in the time-domain. As a result, we have:

$$x_i(t) = \int_{-\infty}^{\infty} d\tau \hat{h}_i(\tau)\hat{d}(\tau + t), \tag{20}$$

where

$$\hat{d}(\tau) = \int_{\infty}^{\infty} df \frac{\tilde{d}(f)}{\sqrt{S_n(|f|)/2}} e^{2\pi i f t} \tag{21}$$

is the whitened data and the whitened template $\hat{h}_i(\tau)$ is defined similarly. Here the accent $\tilde{x}$ represents the corresponding Fourier-transformed frequency of function x and $\hat{y}$ represents the whitened data of the series y. The subscript i represents the process that would run over each set of the template parameters in the template bank. $S_n(f)$ is the single-sided noise power spectral density (PSD).

Gravitational waves generally consist of 2 polarization. Therefore, for each set of parameter in the template bank, there would be 2 real waveforms. One waveform is corresponding to the + polarization and the other one is corresponding to a "quadrature phase-shifted +" waveform which is equal to the $\times$ polarization barring an overall amplitude factor. Now a complex SNR time series $z(t)$ would be able to be constructed with the real part being the + polarized template($x_i(t)$) and the complex part being the "quadrature phase-shifted +" template($y_i(t)$). So that we have

$$z(t) = x_i(t) + iy_i(t). \tag{22}$$

Real-world data collected from the detected often contain glitches from various sources. These glitches would produce high peaks in the SNR time series as the peaks are similar to the waveform at the merger phase. SNR alone is inadequate to distinguish noise from transient signals in presence of non-Gaussian data. To tackle the issue, GstLAL performs a signal consistency test whenever it records an SNR above a certain threshold. ξ^2 is the signal consistency test value. It could be calculated by

$$\xi^2 = \frac{\int_{-\delta t}^{\delta t} dt |z(t) - z(0)R(t)|^2}{\int_{\delta t}^{-\delta t} dt |2 - 2R(t)|^2}, \tag{23}$$

where $z(t)$ is the SNR time series, $z(0)$ is the peak, $R(t)$ is the auto-correlation series and δt is the time window around the peak. The auto-correlation series is calculated by the auto-correlation between the complex template waveform and itself, then scaling it by the peak of the peak complex SNR.

When the GstLAL pipeline records a peak in the SNR time series greater than a preset threshold, it would record the SNR, ξ^2, the masses, and the spins of the templates, which the above values would be returned upon matched filtering, the phase and finally the time of the coalescence. Altogether, these recorded parameters form a trigger. These triggers would then be assigned a log likelihood ratio and the FAP (see the previous section for a more detailed description).

On-going research on searching these sub-threshold lensed counterparts usually focuses on the similarity between the waveform of the possible signals and the confirmed gravitational waves. The sky locations of the incoming waves are not restricted in the searching pipeline. This research aims to modify the terms relating to the sky location restrictions of the signals in the searching pipeline to further increase the accuracy and narrow down the possible candidates to facilitate further analysis of possible gravitationally lensed pairs.

D. Gravitational Lensing

From Einstein's field equation expressed in equation 1, we can see that spacetime is curved around massive objects such as black holes or galaxy clusters. As light travels at the speed of light, it travels in null geodesic such that proper time could not be defined. A new parameter called affine parameter λ could be used in this case. As a result, we can define a velocity like vector

$$\vec{v_\lambda} = \frac{dx}{d\lambda} \tag{24}$$

such that, the geodesic equation

$$\frac{dv^\alpha}{d\tau} = -\Gamma^\alpha_{\mu\nu} v^\mu v^\nu \tag{25}$$

is still valid. By putting equation 24 into equation 25, we can obtain

$$\frac{dv^\alpha_\lambda}{d\tau} = -\Gamma^\alpha_{\mu\nu} v^\mu_\lambda v^\nu_\lambda. \tag{26}$$

By applying equation 26, the paths of light in curved spacetime could be found.

As a toy example, we consider spacetime around spherical celestial bodies using the Schwarschild metric as the majority of the celestial bodies are nearly spherical due to gravity. The Schwarzschild metric is a metric to describe a spherically symmetric curved space-time. Therefore, by substituting the Schwarschild metric in spherical coordinate

$$g_{\mu\nu} = \begin{bmatrix} -(1-\frac{2M}{r}) & 0 & 0 & 0 \\ 0 & (1-\frac{2M}{r})^{-1} & 0 & 0 \\ 0 & 0 & r^2 & 0 \\ 0 & 0 & 0 & r^2 sin^2(\theta) \end{bmatrix} \tag{27}$$

as metric tensor, we can find the Christoffel symbols by using the relation

$$\Gamma^\delta_{\beta\gamma} = \frac{1}{2g_{\alpha\delta}}(\frac{dg_{\alpha\beta}}{dx^\gamma} + \frac{dg_{\alpha\gamma}}{dx^\beta} - \frac{dg_{\beta\gamma}}{dx^\alpha}). \tag{28}$$

Putting equation 28 back to equation 26 would allow us to obtain

$$\frac{dv^r_\lambda}{d\lambda} = (r-3M)(v_\lambda \phi)^2 \tag{29}$$

and

$$v_\lambda \phi \propto \frac{1}{r^2}. \tag{30}$$

Therefore, the path of light around a massive object is bent. In other words, massive objects at or near the path of propagation acts as a "gravitational lens" to bend the propagation direction of lights.

The effect of gravitational lensing predicted by general relativity is illustrated visually in figure 6. As the lights from the source travels through several different paths to reach the observer on Earth, multiple images with different arrival time could be observed.

It is possible to derive the image positions and image brightness using thin lens approximations. The deflection angle α for a light ray passing by a mass M at an impact parameter $b \gg M$ is given by

$$\alpha = \frac{4M}{b} \equiv \frac{2R_S}{b}, \tag{31}$$

where α is the deflection angle, R_S is the Schwarzschild radius, which is equal to

$$R_S = \frac{2M}{c^2}. \tag{32}$$

Besides, all deflection is assumed to be on the normal plane of the line of sight of the gravitational lens. Thin lens approximations could be used with great accuracy as light travels in a straight line in most of the journey except when passing around the gravitational lens. Therefore, we can treat the lens as a point in space, which is the thin lens approximation.

Under thin lens approximation, the bending of light is very subtle. Referring to figure 7, β, θ and α are all very small in reality, as a result, we have

$$\theta D_S = \beta D_S + \alpha D_{LS} \tag{33}$$

, which is called the lens equation. Since $b \approx \xi$ and $\xi \approx \theta D_L$ in the thin lens approximation, equation 33 can be written as

$$\theta = \beta + \frac{\theta_E^2}{\theta}, \tag{34}$$

where

$$\theta_E^2 \equiv \sqrt{2R_S(\frac{D_{LS}}{D_S D_L})} \tag{35}$$

is called the Einstein angle. The solution of equation 34 could be solved to find the angular position of the image I. The solution to equation 34 is

$$\theta\pm = \frac{1}{2}[\beta \pm \sqrt{\beta^2 + 4\theta_E^2}]. \tag{36}$$

It could be observed that 2 images were formed on the same plane, which are on the opposite sides of the position of the

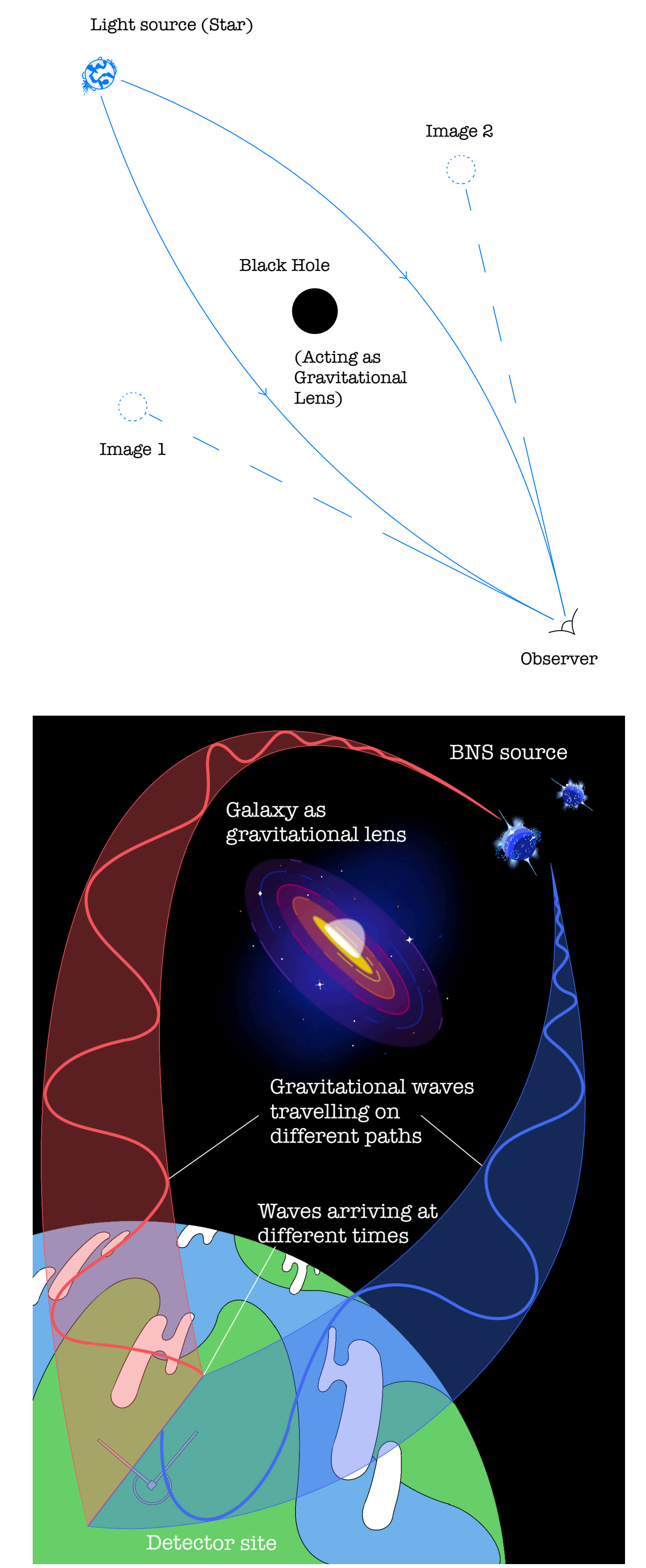

Figure 6. Top: Illustration of the bending of lights around a gravitational lens. In this picture, lights emitted by the star is being lensed by the blackhole situated between the observer and the star. After passing around the blackhole, lights would reach the observer at different angles, so that it would look like there are actually 2 stars located at different positions for the observer. Bottom: Illustration of gravitational lensing of gravitational waves. Gravitational waves from the same source travelling on different paths would produce 2 images with different arrival time and phases.

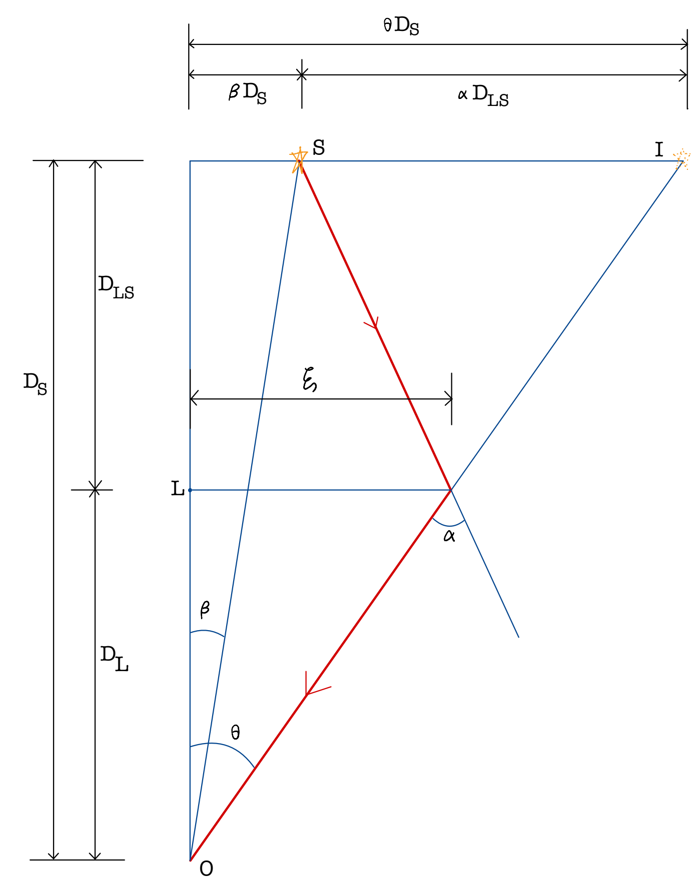

Figure 7. The geometry of gravitational lensing in the thin lens approximation.

lens

By the equivalence principle, since gravitational waves and electromagnetic waves are both waves propagating at the speed of light, the lensing of gravitational waves should have the same effect as electromagnetic waves.

This research would focus on images produced by strong lensing only. The properties of strong lensing include the following

1. Relatively large arrival time difference Δt between images.
2. No overlapping of images due to large Δt and short signal duration of gravitational waves for binary blackhole mergers. Overlapping might occur for binary neutron star mergers as the signal may last for 30 seconds or more [7].
3. Intensity of different images would be different.
4. The amplification factor is frequency-independent (i.e. achromatic), which means all images retain the same waveform although they have different amplitudes.

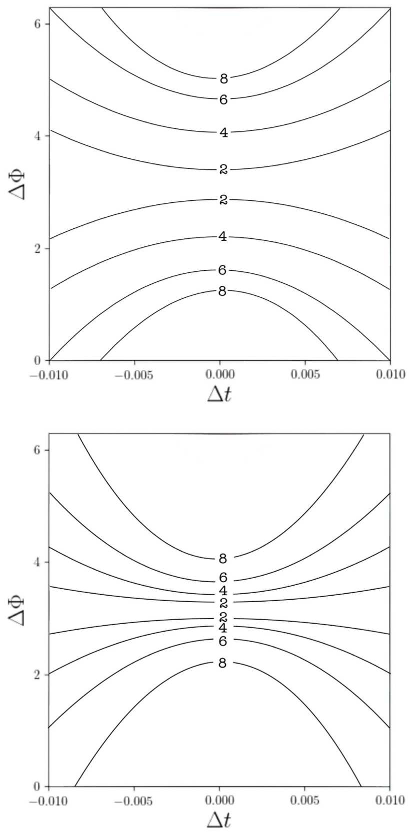

Figure 8. Distribution of $P(\Delta\phi|\Delta t, \rho_{\text{network}})$ modified from [20] (Plot it using computer software later)

.

III. METHOD

The plan to modify the pipeline for lensing searches includes modifying the terms included in calculating the likelihood ratio in equation 17. The 2 terms being modified in the calculation are $\Delta\vec{t}$ and $\Delta\vec{\phi}$. These terms serve the purpose of restricting the sky location of the lensing images. The current sky location uncertainty of the source of the detected gravitational waves is in order of degree [7]. However, the difference in the sky locations of different lensed images is in the order of arc-second [15] which is much smaller than the uncertainty. Therefore, we can assume that different lensed images should come from similar sky locations. By adding the parameters corresponding to the sky locations of the gravitational images, the likelihood ratio would now also consider how likely the 2 gravitational waves came from the same sky location, hence ranking down the candidates that could not be possible to be the lensed counterpart of the detected signal.

Δt is the difference in arrival time of coincident triggers at different detectors [20].Δt for a signal depends only on the position of the source and the location of the observatories. $\Delta\phi$ is the difference in the coalescence phase between H1 and L1 triggers, with $\Delta\phi \in [-\pi, -\pi]$. Therefore, it is obvious that these terms could serve the purpose of restricting sky location. The relationship between Δt, $\Delta\phi$ and the source's sky location is illustrated in figure 9

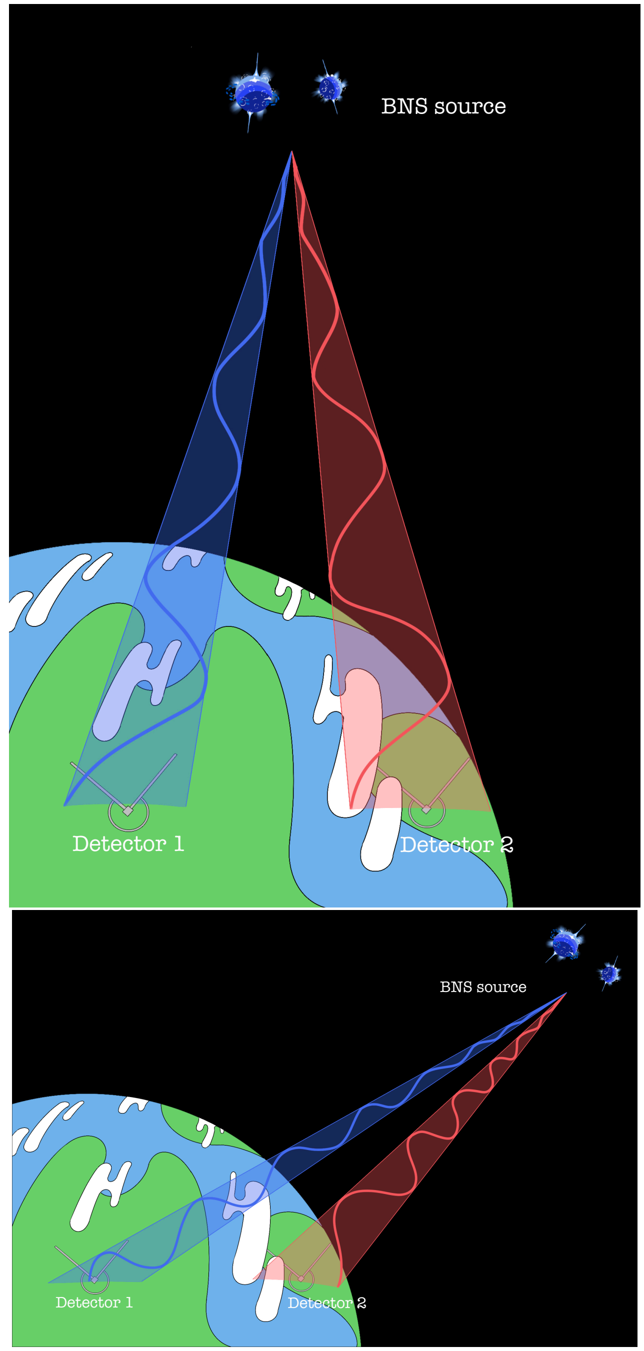

Figure 9. Top: The source is nearly perpendicular to the axis of the 2 detectors. Their arrival times and phases observed by the 2 detectors are nearly identical. Bottom: the source is at an angle to the axis of the detectors. Their arrival time and phases observed by the 2 detectors are different.

We could model the Δt distributions as a function of a ratio of SNRs normalized by horizon distances, to factor out the inherent sensitivities of the detectors, so this term only depends on the position of the source concerning the detectors. Furthermore, we would define it such that it is always smaller than 1,

$$\rho_{\text{ratio}} = \min(\frac{\rho_{H1}/D_{\text{H1}}}{\rho_{L1}/D_{\text{L1}}}, \frac{\rho_{L1}/D_{\text{L1}}}{\rho_{H1}/D_{\text{H1}}}). \quad (37)$$

On the other hand, we do not need to consider the dependence on the detector sensitivities when modeling the $\Delta\phi$ distribution. We only need to consider the dependence of $\Delta\phi$ on Δt and network SNR, which is defined as

$$\rho_{\text{network}} = \sqrt{\rho_1^2 + \rho_2^2}. \quad (38)$$

In figure 8, it shows the logarithm of the probability density function for $P(\Delta\phi|\Delta t, \rho_{\text{network}}, \text{signal})$. The top diagram is the original distribution while the bottom diagram is what the distribution would look like after the modification. As the sky location would be restricted for lensing searches, the contour lines representing $lnP(\Delta\phi|\Delta t, \rho_{\text{network}})$ would be packed significantly closer together. As a result, it would affect the likelihood ratios of the candidates so that we could rank the candidates according to their new likelihood ratios.

To perform the calculation quickly and efficiently, GstLAL employs certain mathematical methods to reduce the computational costs [37]. Firstly, the calculation of the likelihood ratio can be written as

$$\mathcal{L} = \frac{P(\vec{D}_H, \vec{O}, \vec{\rho}, \vec{\xi^2}, \vec{t}, \vec{\phi}|\text{signal})}{P(\vec{D}_H, \vec{O}, \vec{\rho}, \vec{\xi^2}, \vec{t}, \vec{\phi}|\text{noise})}. \quad (39)$$

The numerator can be factorized as with "s" representing "signal"

$$P(\vec{D}_H, \vec{O}, \vec{\rho}, \vec{\xi^2}, \Delta\vec{t}, \Delta\vec{\phi}|\text{s}) = P(\vec{D}_H|\text{s}) \times P(\vec{O}|\vec{D}_H, \text{s}) \times P(\vec{\xi^2}|\vec{\rho}, \text{s}) \times P(\vec{\rho}, \vec{\phi}, \vec{t}|\vec{O}, \vec{D}_H, \text{s}). \quad (40)$$

By replacing ρ with effective distances $\vec{D}_{eff} =$, we have

$$P(\vec{\rho}, \vec{\phi}, \vec{t}|\vec{O}, \vec{D}_H, \text{s}) \propto P(ln\Delta\vec{D}_{eff}, \Delta\vec{\phi}, \Delta\vec{t}|\vec{O}, \text{s}) \times |\rho|^{-4}. \quad (41)$$

To simplify the situation, we can define a vector $\vec{\lambda}$ such that

$$\vec{\lambda} \equiv [\Delta ln\vec{D}_{eff}, \Delta\vec{\phi}, \Delta\vec{t}]. \quad (42)$$

In order to construct the distribution of these parameters for a signal, a uniform distribution of gravitational waves in Earth-based coordinates was asserted. They are, namely: right ascension α, declination $\cos(\delta)$, inclination angle $\cos(\iota)$, and polarization angle Φ. A uniform, densely sampled grid in $[\alpha, \cos(\delta), \cos(\iota), \cos(\delta)]$ could be formed and further assert that any signal should "exactly" land on one of the grid points. The grid is then transformed to a grid of irregularly spaced points in $\vec{\lambda}$, which is denoted as $\vec{\lambda}_{mi}$ for the i^{th} model vector.

After using covariance matrix, Fisher information matrix, and Cholesky decomposition for simplifications, the probability distribution now becomes

$$P(\lambda|\vec{O}, \text{s}) \approx exp[-\frac{1}{2}\vec{\Delta x}_0^2] \times \Sigma_i exp[-\frac{1}{2}g_{0i}^2], \quad (43)$$

where $\vec{\Delta x}_0$ refers to the distance between the candidate parameter and the nearest-neighbour grid point, and g_{0i} is the distance between the i^{th} grid point to the nearest grid point. Since the entire sum over i term can be precomputed and stored, it would allow a fast and efficient evaluation during the observing runs.

IV. WORK PLAN

Date	Task
15^{th} May 2022	Finish and Submit Project Proposal
14^{th} June 2022	Start of LIGO SURF 2022
5-11^{th} July 2022	Finish and Submit Interim Report 1
26^{th} July - 1^{st} August 2022	1. Submit Interim Report 2 2. Submit Abstract
18 - 19^{th} August 2022	Final Presentation
4^{th} September 2022	Finish and Submit Final Report

V. REFERENCES

[1] A. Einstein, Sitzungsber. Preuss. Akad. Wiss. Berlin (Math. Phys.) **1915**, 778 (1915), [Addendum: Sitzungsber.Preuss.Akad.Wiss.Berlin (Math.Phys.) 1915, 799–801 (1915)].

[2] B. P. Abbott *et al.* (LIGO Scientific, Virgo), Phys. Rev. Lett. **116**, 061102 (2016), arXiv:1602.03837 [gr-qc].

[3] R. Abbott *et al.* (LIGO Scientific, VIRGO, KAGRA), (2021), arXiv:2111.03634 [astro-ph.HE].

[4] B. P. Abbott *et al.* (LIGO Scientific, Virgo), Phys. Rev. X **9**, 031040 (2019), arXiv:1811.12907 [astro-ph.HE].

[5] R. Abbott *et al.* (LIGO Scientific, Virgo), Phys. Rev. X **11**, 021053 (2021), arXiv:2010.14527 [gr-qc].

[6] R. Abbott *et al.* (LIGO Scientific, VIRGO, KAGRA), (2021), arXiv:2111.03606 [gr-qc].

[7] B. P. Abbott *et al.* (LIGO Scientific, Virgo), Phys. Rev. Lett. **119**, 161101 (2017), arXiv:1710.05832 [gr-qc].

[8] B. T. Reed, A. Deibel, and C. J. Horowitz, Astrophys. J. **921**, 89 (2021), arXiv:2104.00771 [astro-ph.HE].

[9] N. Andersson, Universe **7**, 97 (2021), arXiv:2103.10223 [gr-qc].

[10] F. Pretorius and W. E. East, Phys. Rev. D **98**, 084053 (2018), arXiv:1807.11562 [gr-qc].
[11] T. Nakama, J. Silk, and M. Kamionkowski, Phys. Rev. D **95**, 043511 (2017), arXiv:1612.06264 [astro-ph.CO].
[12] A. I. Renzini, B. Goncharov, A. C. Jenkins, and P. M. Meyers, Galaxies **10**, 34 (2022), arXiv:2202.00178 [gr-qc].
[13] B. P. Abbott *et al.* (LIGO Scientific, Virgo, VIRGO), Astrophys. J. **909**, 218 (2021), [Erratum: Astrophys.J. 923, 279 (2021)], arXiv:1908.06060 [astro-ph.CO].
[14] B. P. Abbott *et al.* (LIGO Scientific, Virgo, 1M2H, Dark Energy Camera GW-E, DES, DLT40, Las Cumbres Observatory, VINROUGE, MASTER), Nature **551**, 85 (2017), arXiv:1710.05835 [astro-ph.CO].
[15] J. B. Hartle, *Gravity* (Cambridge University Press, 2021).
[16] T. Broadhurst, J. M. Diego, and G. F. Smoot, (2019), arXiv:1901.03190 [astro-ph.CO].
[17] L. Dai, B. Zackay, T. Venumadhav, J. Roulet, and M. Zaldarriaga, (2020), arXiv:2007.12709 [astro-ph.HE].
[18] L. P. Singer, D. A. Goldstein, and J. S. Bloom, (2019), arXiv:1910.03601 [astro-ph.CO].
[19] R. Abbott *et al.* (LIGO Scientific, VIRGO), Astrophys. J. **923**, 14 (2021), arXiv:2105.06384 [gr-qc].
[20] S. Sachdev *et al.*, (2019), arXiv:1901.08580 [gr-qc].
[21] F. Aubin *et al.*, Class. Quant. Grav. **38**, 095004 (2021), arXiv:2012.11512 [gr-qc].
[22] Q. Chu *et al.*, Phys. Rev. D **105**, 024023 (2022), arXiv:2011.06787 [gr-qc].
[23] S. A. Usman *et al.*, Class. Quant. Grav. **33**, 215004 (2016), arXiv:1508.02357 [gr-qc].
[24] A. Einstein, Annalen Phys. **17**, 891 (1905).
[25] B. P. Abbott *et al.* (LIGO Scientific, Virgo, Fermi-GBM, INTEGRAL), Astrophys. J. Lett. **848**, L13 (2017), arXiv:1710.05834 [astro-ph.HE].
[26] "What is an interferometer?" .
[27] "Ligo technology," ().
[28] "Ligo's interferometer," ().
[29] "Ligo's laser," ().
[30] "Vibration isolation," ().
[31] A. Buikema *et al.* (aLIGO), Phys. Rev. D **102**, 062003 (2020), arXiv:2008.01301 [astro-ph.IM].
[32] "Ligo optics," ().
[33] J. D. E. Creighton and W. G. Anderson, *Gravitational-wave physics and astronomy: An introduction to theory, experiment and data analysis* (2011).
[34] A. K. Y. Li, R. K. L. Lo, S. Sachdev, C. L. Chan, E. T. Lin, T. G. F. Li, and A. J. Weinstein, (2019), arXiv:1904.06020 [gr-qc].
[35] J. Janquart, O. A. Hannuksela, H. K., and C. Van Den Broeck, Mon. Not. Roy. Astron. Soc. **506**, 5430 (2021), arXiv:2105.04536 [gr-qc].
[36] C. Messick *et al.*, Phys. Rev. D **95**, 042001 (2017), arXiv:1604.04324 [astro-ph.IM].
[37] C. Hanna *et al.*, Phys. Rev. D **101**, 022003 (2020), arXiv:1901.02227 [gr-qc].